Editors' Suggestion | Featured in Physics

Instability-Induced Pattern Formations in Soft Magnetoactive Composites

Artemii Goshkoderia,[1] Vincent Chen,[2,3] Jian Li,[4] Abigail Juhl,[2] Philip Buskohl,[2] and Stephan Rudykh[5,*]
[1]Department of Aerospace Engineering, Technion—Israel Institute of Technology, Haifa 32000, Israel
[2]Air Force Research Laboratory, Wright-Patterson AFB, Ohio 45433-7718, USA
[3]UES, Inc., Dayton, Ohio 45432, USA
[4]Department of Civil and Environmental Engineering, Massachusetts Institute of Technology, Cambridge, Massachusetts 02138, USA
[5]Department of Mechanical Engineering, University of Wisconsin–Madison, Madison, Wisconsin 53706, USA

(Received 17 December 2018; revised manuscript received 21 November 2019; accepted 4 March 2020; published 14 April 2020)

Elastic instabilities can trigger dramatic microstructure transformations giving rise to unusual behavior in soft matter. Motivated by this phenomenon, we study instability-induced pattern formations in soft magnetoactive elastomer (MAE) composites deforming in the presence of a magnetic field. We show that identical MAE composites with periodically distributed particles can switch to a variety of new patterns with different periodicity upon developments of instabilities. The newly formed patterns and postbuckling behavior of the MAEs are dictated by the magnitude of the applied magnetic field. We identify the particular levels of magnetic fields that give rise to strictly doubled or multiplied periodicity upon the onset of instabilities in the periodic particulate soft MAE. Thus, the predicted phenomenon can be potentially used for designing new reconfigurable soft materials with tunable material microstructures remotely controlled by a magnetic field.

DOI: 10.1103/PhysRevLett.124.158002

Soft active materials can undergo reversible shape transformations induced by external stimuli such as light [1], heat [2], electric [3], or a magnetic field [4]. Magnetoactive elastomers (MAEs)—a class of soft active materials that respond to magnetic field excitation—have attracted significant attention due to their simple, remote, and reversible principle of actuation. Potential applications include remotely controlled actuators [4,5], variable-stiffness devices [6,7], tunable vibration absorbers [8–10] and damping components [11,12], noise barrier system [13,14], and sensors [15] among others. MAEs are composite materials that consist of magnetizable particles embedded in a soft matrix material. Typically, a polymeric matrix material in its liquid state prior to polymerization is mixed with magnetizable particles (of micro or even nano size) [16]. The presence of the magnetic field results in the formation of chainlike structures aligned along the direction of the magnetic field applied during curing. Through this microstructure modification, different interactions between magnetizable particles are induced, thus, enabling tunability of the overall magnetomechanical behavior of MAEs. Moreover, highly structured soft magnetoactive material can be designed to capitalize on local buckling or *instability* phenomenon triggering dramatic changes in material microstructures and, thus, reversible switches in material properties.

Historically, instability phenomenon or buckling was considered as a limiting factor associated with failure. Recently, however, the instability phenomenon has been embraced for designing new materials with unusual properties, switchable microstructures, and functions. Elastic instabilities give rise to sudden changes in microstructures [17] that can be leveraged for designing materials with negative Poisson's ratio behavior [18–22], shape-morphing abilities [23], tunable stiffness [24], controllable surface properties (adhesion and wettability) [25], tunable color [26], and phononic [27–30] and photonic [31] switches. Moreover, buckling-induced microstructure transformations [17] are frequently observed in nature [32] and have been employed to enable new actuation mechanisms [33,34] for soft robotics. These systems, however, require direct mechanical loading to induce the transformations and gain access to instability-induced unusual properties and behaviors. Here, we explore the phenomenon when the energy is supplied remotely by the application of an external magnetic field.

In this Letter, we specifically focus on the instability phenomenon and associated pattern transformations in soft magnetoactive materials undergoing large deformations in the presence of a magnetic field. To this end, we perform a numerical analysis of the postbuckling behavior of a MAE with rigid magnetizable inclusions periodically distributed in a soft matrix. Long-wave or macroscopic instabilities [35,36] can be predicted through the effective behavior of various homogenization schemes [36–38]. However, instabilities can develop at smaller length scales comparable with the characteristic length of the microstructure (see [39,40] for the analogous case of dielectric elastomer laminates). Because of the complexity of MAE nonlinear behavior and composite architecture, there is very limited

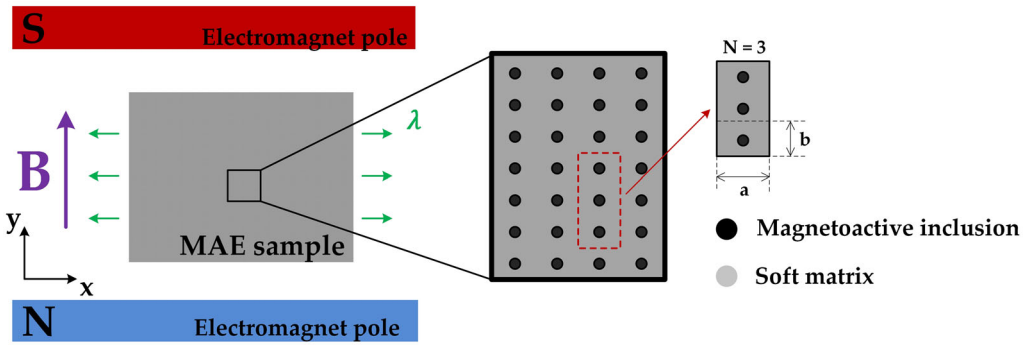

FIG. 1. Schematic representation of MAE composite with rectangular unit cells subjected to a vertically applied magnetic field and horizontally applied prestress. Each unit cell is comprised of soft matrix and centered magnetoactive inclusion. An example of representative volume element (RVE) containing $N = 3$ unit cells (right).

knowledge about instabilities in these soft active materials [35,36,41,42], and even less is known about their post-instability behavior.

In this study, we investigate the postbuckling behavior of periodic MAE composites with circular inclusions periodically distributed in a soft matrix. Through our computations, we numerically realize the formation and evolution of new patterns in the postbuckling regime in the periodic MAE. We analyze the influence of the magnetic field on instability-induced new patterns. We find that, under the excitation by the magnetic field of specific levels, the MAE experiences a predesigned reconfiguration of the microstructures and formations of distinct strictly periodic patterns.

Consider MAE composites with periodically distributed stiff magnetizable particles embedded in a soft matrix. A schematic illustration of a periodically structured MAE composite with a rectangular periodic unit cell with circular inclusions is shown in Fig. 1. Geometrically, the microstructure is characterized by the initial periodicity aspect ratio $\eta = a/b$, the inclusion spacing ratio $\xi = d/b$, and magnetizable inclusion volume fraction $c = \pi d^2/4ab$, where d is the inclusion diameter.

The equilibrium equation in the absence of body forces is

$$\mathrm{div}\boldsymbol{\sigma} = \mathbf{0}, \tag{1}$$

where $\boldsymbol{\sigma}$ is the *total* Cauchy stress (including elastic and magnetically induced stresses) tensor with the symmetry $\boldsymbol{\sigma}^T = \boldsymbol{\sigma}$. The magnetostatic Maxwell equations in the absence of surface and free currents reduce to

$$\mathrm{div}\mathbf{B} = 0 \quad \text{and} \quad \mathrm{curl}\mathbf{H} = \mathbf{0}, \tag{2}$$

where $\mathbf{B}$ is the magnetic field and $\mathbf{H}$ is the magnetic field intensity in the deformed configuration; these are related as $\mathbf{B} = \mu_0(\mathbf{H} + \mathbf{M})$, where $\mathbf{M}$ is the magnetization and μ_0 is the free space permeability.

The corresponding phase energy potentials are expressed in terms of elastic and magnetic parts $\Psi = \Psi^{(\mathrm{el})} + \Psi^{(\mathrm{mag})}$; in particular, an augmented neo-Hookean nonlinear materials model is employed [43] (see Supplemental Material [44] for details). For magnetizable particles, a Langevin form of the magnetic energy potential is used:

$$\rho\Phi = \frac{\mu_0 m_s^2}{3\chi}\left[\ln\left(\sinh\left[\frac{3\chi|\mathbf{B}|}{\mu_0 m_s}\right]\right) - \ln\left(\frac{3\chi|\mathbf{B}|}{\mu_0 m_s}\right)\right], \tag{3}$$

where ρ is the inclusion phase density.

To analyze the instability-induced pattern formations and the behavior in the postbuckling regime, a nonlinear analysis has been performed through the finite element simulations. In our model, we assign the initial matrix shear modulus as $G^{(m)} = 50$ kPa, while the particles are assumed to be 1000 times stiffer with the shear modulus $G^{(i)}/G^{(m)} = 10^3$, thus leading to nearly rigid behavior of the inclusions. The initial susceptibility and saturation magnetization of the particles are $\chi = 0.995$ and $m_s = 0.77$ T, respectively. Since magnetoelastic instabilities may lead to the formation of new periodicity, updated representative volume elements (RVEs) were constructed containing various numbers of the original unit cell N. The material is subjected to a magnetic field applied in the y direction, and it is compressed in the same direction as shown in Fig. 1. The applied compressive strain ϵ_y can be expressed in terms of horizontal stretch ratio λ as $\epsilon = \epsilon_y = 1 - \lambda^{-1}$, if the material is assumed to be incompressible. For later use, we introduce here the normalized magnetic field $\tilde{B} = B/\sqrt{\mu_0 G^{(m)}}$ [45] and the dimensionless stress component $\tilde{\sigma}_{yy} = \tilde{B}^2/2 - \sigma_{yy}/G^{(m)}$ [46]. Note that a magnetomechanical loading path is defined in the two-dimensional space of $\tilde{B}$ and ϵ [see Fig. 3(b)]. There is an infinite number of paths (combinations of $\tilde{B}$ and ϵ) leading to the identical buckling point in the two-dimensional space. The instability analysis is described in Supplemental Material [44].

We illustrate the formation of new periodic and quasi-periodic patterns due to instabilities in the periodic MAEs for various magnetic fields applied along the particle chain direction in Fig. 2. The examples are given for periodic

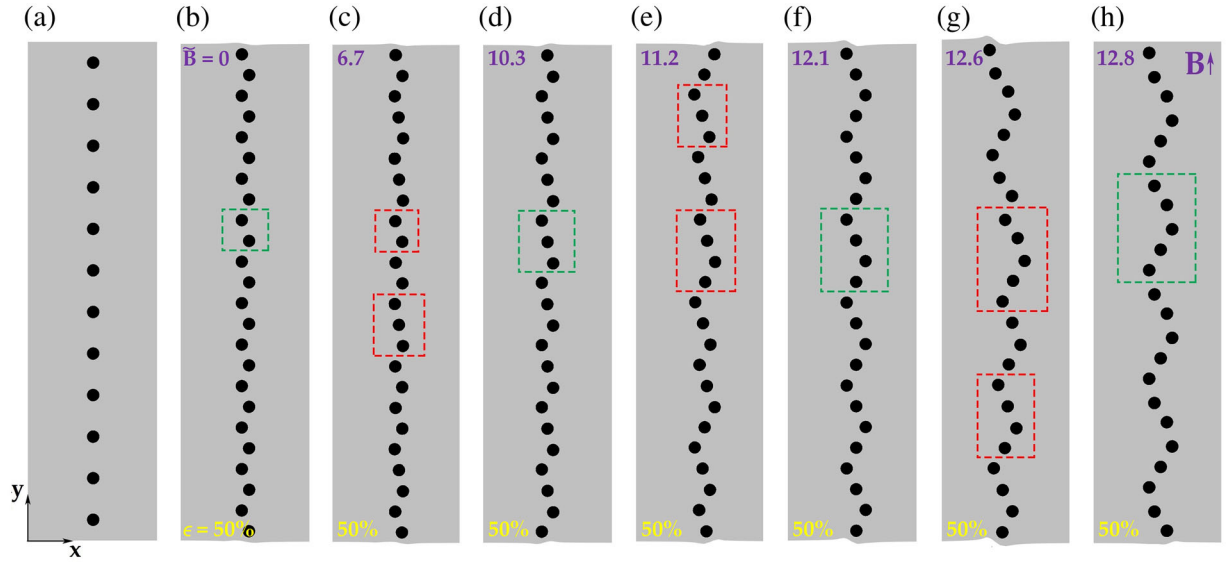

FIG. 2. Numerically realized instability-induced periodic (b),(d),(f),(h) and nonperiodic (c),(e),(g) patterns in soft MAE composites at $\epsilon = 50\%$ [47] and various levels of $\tilde{B} = 0$, 6.7, 10.3, 11.2, 12.1, 12.6, 12.8 (b)–(d). (a) Undeformed state. The elements of strictly periodic patterns $N_p = 2$ (b), $N_p = 3$ (d), $N_p = 4$ (f), and $N_p = 5$ (h) are marked by green dashed rectangles, and base elements of nonperiodic $N_b = 2$, 3 (c), $N_b = 3$, 4 (e), and $N_b = 4$, 5 (g) patterns are denoted by red dashed rectangles.

MAEs with $\eta = 5$ (see Fig. 1) and $\xi = 0.309$. The compressive strain level was gradually increased up to $\epsilon = 50\%$ while $\tilde{B}$ was kept fixed. Upon achieving the critical strain corresponding to instabilities [$\epsilon_c = 46.8\%$ (b), 46.9% (c), 42.8% (d), 43.2% (e), 37.9% (f), 35.3% (g), and 34.4% (h)], particles cooperatively rearrange into new patterns. Figure 2(b) shows that the soft composite deformed at $\tilde{B} = 0$ switches into the new pattern characterized by particle pairing forming a new doubled periodicity. The application of a magnetic field leads to the formation of distinct patterns depending on the values of $\tilde{B}$. Thus, for example, new patterns with increased periodicity $N_p = 3$ (d), 4 (f), and 5 (h) form [48], when the MAE is subjected to $\tilde{B} = 10.3$ (d), 12.1 (f), and 12.8 (h). The corresponding normalized buckling stresses for periodic patterns are $\tilde{\sigma}_{yy} = 0.8$ (b), 0.869 (d), 0.863 (f), and 0.846 (h). We observe that the periodicity (or wavelength) of the patterns increases as $\tilde{B}$ increases. Note that the increase in $\tilde{B}$ leads to the evolution of the microstructure toward cooperative particle formation into wavy patterns [compare, for example, Figs. 2(b) and 2(h)]. We observe that only narrow ranges of the specific levels of $\tilde{B}$ give rise to the formation of the strictly periodic patterns. For the transition level of the magnetic field, the instability-induced patterns are characterized by formations of quasiperiodic patterns with irregularly repeating base elements. The size of the irregular, repeating patterns ranged from two, three, four, or five particles, depending on the level of $\tilde{B}$. Examples of such instability-induced irregular quasiperiodic patterns are shown in Figs. 2(c), 2(e), and 2(g).

The dependence of ϵ_c on $\tilde{B}$ is shown in Fig. 3. The circles correspond to the reported pattern formations, while the dashed curve connecting the points is given for indicating the trend of $\epsilon_c = \epsilon_c(\tilde{B})$ dependence. The continuous curve represents the prediction for long-wave or macroscopic instabilities. This is calculated through the analysis of the effective (or homogenized) responses of the MAE composites; in particular, a criterion for loss of elliptic ity has been utilized [36]. Although the long-wave instability analysis predicts similar trends, we note that microscopic instabilities develop earlier—at lower ϵ_c as compared to the

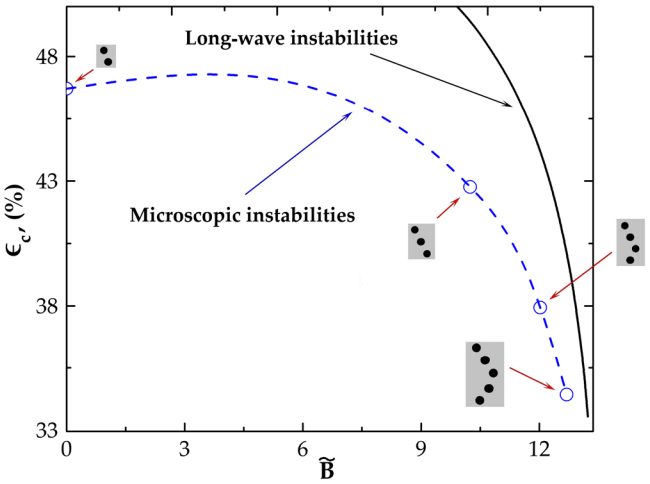

FIG. 3. Dependence of critical strain on the applied magnetic field level. The numerically detected critical buckling points are denoted by circles corresponding to the periodic patterns from Figs. 2(b), 2(d), 2(f), and 2(h), and the connecting dashed curve illustrates the trend of the dependence of critical strain on the magnetic field. The continuous curve represents the long-wave instability prediction.

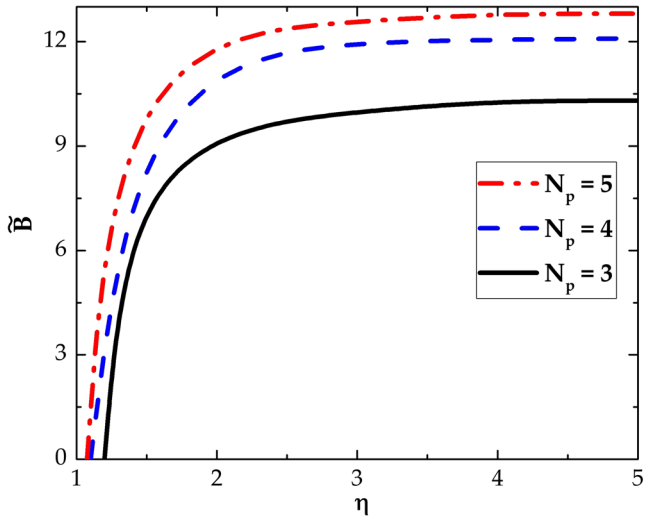

FIG. 4. Dependence of the critical magnetic field required for the formation of the periodic patterns on η ($\xi = 0.309$). Continuous, dashed, and dash-dotted curves correspond to periodic patterns with $N_p = 3$, 4, and 5, respectively.

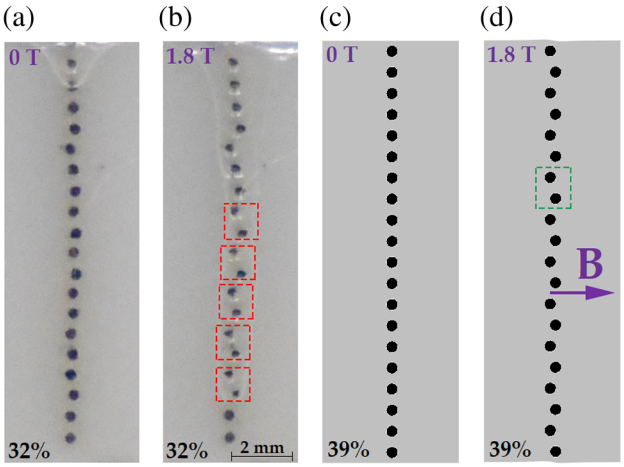

FIG. 5. Magnetic field triggers instability-induced patterns in soft MAE composites. (a),(b) Experimentally observed patterns for the applied compressive strain level 32% and for the magnetic fields $B = 0$ (a) and $B = 1.8$ T (b), respectively. (c),(d) Numerically realized patterns for the applied compressive strain level 39% and for $B = 0$ (c) and $B = 1.8$ T (d), respectively. The magnetic field is applied perpendicularly to the inclusion column direction.

long-wave estimates. The difference in the corresponding values of ϵ_c is more significant in the weak magnetic field regime, whereas at high values of $\tilde{B}$, these curves approach each other, and long-wave analysis provides reasonable estimates for instabilities. Once the macroscopic instability regime is attained (for example, at high values of $\tilde{B}$), a rapid increase in the buckling wavelength is expected; this transition from micro- to macroscopic instabilities manifests in high ratios between the buckling wavelength and the microstructure characteristic size (single-particle unit cell).

Figure 4 shows the dependence of the critical magnetic field–required for the formation of the *periodic* patterns–on periodicity ratio η for a fixed $\xi = 0.309$. Continuous, dashed, and dash-dotted curves correspond to the periodic patterns with $N_p = 3$, 4, and 5, respectively. We observe that, to induce the formation of the patterns with higher periodicities, high values of $\tilde{B}$ are required. For small η, when the particle columns are relatively close, the critical magnetic field depends strongly on η; however, as the distance between the columns is increased, the dependence saturates and $\tilde{B}$ asymptotically approaches the value corresponding to a single-column MAE. The high sensitivity of particle periodicity to small changes in η, in the small η regime, will likely inhibit uniform periodicity in the experimental system due to geometric defects introduced during fabrication. We note that strictly periodic structures form in the vicinity of the N_p curves; however, these regions are rather narrow, and quasiperiodic patterns emerge for $\tilde{B}$ in the ranges between the curves and below the black continuous curve.

Finally, we probe the idea in an experimental setup on a MAE composite sample. The sample is comprised of 19 steel rods (with ~80% iron content) embedded in a silicon rubber matrix ($G^{(m)} = 107$ kPa). The MAE sample is placed between the poles of an electromagnet, and then it is prestrained in the presence of the magnetic field of various levels. Note that, due to the experimental limitations, the magnetic field is applied perpendicularly to the prestrain direction. Details regarding the sample preparation and experiments are given in Supplemental Material [44]. Figure 5 shows the experimental [(a),(b)] and numerical [(c),(d)] postbuckling patterns in the MAE composite. In modeling, we use $G^{(m)} = 107$ kPa for the matrix, and $\chi = 0.995$ and $\mu_0 m_s = 2$ T for the rigid magnetizable particles. The composite is subjected to magnetic fields $B = 0$ T [(a),(c)] and $B = 1.8$ T [(b),(d)] and compressive strain levels 32% [(a),(b)] and 39% [(c),(d)], respectively. The structure spacing ratio is $\xi = 0.68$ corresponding to the periodic postbuckling pattern in the absence of a magnetic field. The experiments show that the postbuckling pattern is characterized by a higher amplitude when the magnetic field is applied (b) as compared to purely mechanical loading (a). Moreover, the application of the magnetic field transforms the postbuckling configuration of the particles. The nonperiodic pattern (a) attains the periodic configuration (b) when the magnetic field is applied. The repeating base elements $N_b = 2$ denoted by red rectangles are shown in Fig. 5(b). Figures 5(c) and 5(d) show the numerical simulations also capturing the magnetic-field-induced increase in the amplitude. The observed amplitude change is due to the fact that the composite buckles earlier when a magnetic field is applied perpendicularly to the column. Note that this behavior is similar to the case of the magnetic

excitation applied along the column [see Fig. 3(a)]. The numerical critical strains are higher for both $B = 0$ T (buckles at $\epsilon_{cr} = 44\%$) and $B = 1.8$ T ($\epsilon_{cr} = 39\%$) as compared to the experiments. The discrepancy between the numerical and experimental buckling strains can stem from various factors, such as initial geometrical imperfections in the tested samples, edge effects, and inelastic behavior of the soft matrix.

In summary, we found instability-induced patterns—that are inadmissible in the absence of a magnetic field—in soft magnetosensitive periodic systems of rigid magnetizable particles distributed periodically in a soft magnetically inactive matrix. We observed that the magnetizable particles rearrange in a cooperative manner into new configurations depending on the applied magnetic field. Moreover, under the action of certain magnetic fields, fully determined and strictly periodic structures are formed. The magnitudes of the required critical magnetic field are sensitive to a change in spacing between the inclusion columns: the effect is strong for smaller distances, but the dependence quickly saturates to the single-column value as the spacing is increased. The corresponding critical strain was found to decrease with an increase in the magnetic field; interestingly, this trend is similar to the one predicted by long-wave magnetomechanical stability analysis based on the effective behavior of the soft MAEs. Note that the buckling point is independent of the magnetomechanical loading path. In the postbuckling regime, however, secondary bifurcations and associated distinct pattern transformations are possible for different loading paths. We hope that our results for instability-induced pattern formations will motivate further theoretical and experimental studies of the phenomenon. We note that the behavior of the systems is highly sensitive to imperfections, thus posing challenges in fabrication of the highly structured materials. Potentially, the periodic MAE systems can be produced through various 3D printing techniques [4,14,49] across the length scales. On the other hand, imperfections or defects can be tailored to achieve different microstructures with distinct properties.

These findings can open new ways for designing switchable behavior in soft matter with applications ranging from soft phononics and wave propagation manipulation to remotely controlled soft microactuators. For example, magnetically induced instabilities can be used by trigger auxetic behavior, thus allowing the material or robot to squeeze through a narrow space and then regain the original shape and function. In addition, the local-microstructural transformations can be activated inhomogeneously such that global motions can be exerted on account of the inhomogeneously distributed local buckling. Remarkably, the application of a magnetic field can turn periodic microstructures into *quasiperiodic* ones. This could be used for designing systems with quasicrystal-like structures [50–52] that are not admissible mechanically. These switchable material systems may be of interest for developing metamaterials and the exploration of the wave propagation phenomenon. Moreover, the ideas can be extended to broader classes of materials, including soft dielectric elastomers [53,54] and materials with predesigned incompatibilities through 3D printing [55].

The research was partially supported by the Air Force Office of Scientific Research under the research tasks 17RXCOR435 and FA8655-20-1-7003 though Project No. 19IOE010 and by the European Research Council (ERC) under the European Union's Horizon 2020 research and innovation programme (Grant No. 852281 - MAGIC).

*rudykh@wisc.edu

[1] S. Palagi, A. G. Mark, S. Y. Reigh, K. Melde, T. Qiu, H. Zeng, C. Parmeggiani, D. Martella, A. Sanchez-Castillo, N. Kapernaum *et al.*, Structured light enables biomimetic swimming and versatile locomotion of photoresponsive soft microrobots, Nat. Mater. **15**, 647 (2016).

[2] M. Behl and A. Lendlein, Actively moving polymers, Soft Matter **3**, 58 (2007).

[3] E. Acome, S. Mitchell, T. Morrissey, M. Emmett, C. Benjamin, M. King, M. Radakovitz, and C. Keplinger, Hydraulically amplified self-healing electrostatic actuators with muscle-like performance, Science **359**, 61 (2018).

[4] Y. Kim, H. Yuk, R. Zhao, S. A. Chester, and X. Zhao, Printing ferromagnetic domains for untethered fast-transforming soft materials, Nature (London) **558**, 274 (2018).

[5] S.-Y. Tang, X. Zhang, S. Sun, D. Yuan, Q. Zhao, S. Yan, L. Deng, G. Yun, J. Zhang, S. Zhang *et al.*, Versatile microfluidic platforms enabled by novel magnetorheological elastomer microactuators, Adv. Funct. Mater. **28**, 1705484 (2018).

[6] Z. Varga, G. Filipcsei, and M. Zrinyi, Smart composites with controlled anisotropy, Polymer **46**, 7779 (2005).

[7] R. M. Erb, R. Libanori, N. Rothfuchs, and A. R. Studart, Composites reinforced in three dimensions by using low magnetic fields, Science **335**, 199 (2012).

[8] J. M. Ginder, W. F. Schlotter, and M. E. Nichols, Magnetorheological elastomers in tunable vibration absorbers, Proc. SPIE Int. Soc. Opt. Eng. **4331**, 103 (2001).

[9] H. Deng, X. Gong, and L. Wang, Development of an adaptive tuned vibration absorber with magnetorheological elastomer, Smart Mater. Struct. **15**, N111 (2006).

[10] Q. Wang, X. Dong, L. Li, and J. Ou, Mechanical modeling for magnetorheological elastomer isolators based on constitutive equations and electromagnetic analysis, Smart Mater. Struct. **27**, 065017 (2018).

[11] X. Gong, Y. Fan, S. Xuan, Y. Xu, and C. Peng, Control of the damping properties of magnetorheological elastomers by using polycaprolactone as a temperature-controlling component, Ind. Eng. Chem. Res. **51**, 6395 (2012).

[12] J. Yang, X. Gong, H. Deng, L. Qin, and S. Xuan, Investigation on the mechanism of damping behavior of magnetorheological elastomers, Smart Mater. Struct. **21**, 125015 (2012).

[13] M. Farshad and M. Le Roux, A new active noise abatement barrier system, Polymer Testing **23**, 855 (2004).
[14] K. Yu, N. X. Fang, G. Huang, and Q. Wang, Magnetoactive acoustic metamaterials, Adv. Mater. **30**, 1706348 (2018).
[15] T. F. Tian, W. H. Li, and Y. M. Deng, Sensing capabilities of graphite based mr elastomers, Smart Mater. Struct. **20**, 025022 (2011).
[16] M. R. Jolly, J. D. Carlson, and B. C. Munoz, A model of the behavior of magnetorheological materials, Smart Mater. Struct. **5**, 607 (1996).
[17] T. Mullin, S. Deschanel, K. Bertoldi, and M. C. Boyce, Pattern Transformation Triggered by Deformation, Phys. Rev. Lett. **99**, 084301 (2007).
[18] K. Bertoldi, P. M. Reis, S. Willshaw, and T. Mullin, Negative Poisson's ratio behavior induced by an elastic instability, Adv. Mater. **22**, 361 (2010).
[19] S. Babaee, J. Shim, J. C. Weaver, E. R. Chen, N. Patel, and K. Bertoldi, 3d soft metamaterials with negative poisson's ratio, Adv. Mater. **25**, 5044 (2013).
[20] B. Florijn, C. Coulais, and M. van Hecke, Programmable Mechanical Metamaterials, Phys. Rev. Lett. **113**, 175503 (2014).
[21] J. Li, V. Slesarenko, and S. Rudykh, Auxetic multiphase soft composite material design through instabilities with application for acoustic meta- materials, Soft Matter **14**, 6171 (2018).
[22] M. J. Frazier and D. M. Kochmann, Atomimetic mechanical structures with nonlinear topological domain evolution kinetics, Adv. Mater. **29**, 1605800 (2017).
[23] A. Rafsanjani and K. Bertoldi, Buckling-Induced Kirigami, Phys. Rev. Lett. **118**, 084301 (2017).
[24] G. McKnight and C. Henry, Large strain variable stiffness composites for shear deformations with applications to morphing aircraft skins, Proc. SPIE Int. Soc. Opt. Eng. **6929**, 692919 (2008).
[25] S. Singamaneni and V. V. Tsukruk, Buckling instabilities in periodic composite polymeric materials, Soft Matter **6**, 5681 (2010).
[26] J. Li, J. Shim, J. Deng, J. T. Overvelde, X. Zhu, K. Bertoldi, and S. Yang, Switching periodic membranes via pattern transformation, and shape memory effect, Soft Matter **8**, 10322 (2012).
[27] K. Bertoldi and M. C. Boyce, Wave propagation and instabilities in monolithic and periodically structured elastomeric materials undergoing large deformations, Phys. Rev. B **78**, 184107 (2008).
[28] P. Wang, F. Casadei, S. Shan, J. C. Weaver, and K. Bertoldi, Harnessing Buckling to Design Tunable Locally Resonant Acoustic Metamaterials, Phys. Rev. Lett. **113**, 014301 (2014).
[29] S. Rudykh and M. Boyce, Transforming Wave Propagation in Layered Media Via Instability-Induced Interfacial Wrinkling, Phys. Rev. Lett. **112**, 034301 (2014).
[30] C. Gao, V. Slesarenko, M. C. Boyce, S. Rudykh, and Y. Li, Instability-induced pattern transformation in soft metamaterial with hexagonal networks for tunable wave propagation, Sci. Rep. **8**, 11834 (2018).
[31] D. Krishnan and H. Johnson, Optical properties of two-dimensional polymer photonic crystals after deformation-induced pattern transformations, J. Mech. Phys. Solids **57**, 1500 (2009).
[32] A. J. Crosby, Why should we care about buckling?, Soft Matter **6**, 5660 (2010).
[33] D. Yang, B. Mosadegh, A. Ainla, B. Lee, F. Khashai, Z. Suo, K. Bertoldi, and G. M. Whitesides, Buckling of elastomeric beams enables actuation of soft machines, Adv. Mater. **27**, 6323 (2015).
[34] T. Chen, O. R. Bilal, K. Shea, and C. Daraio, Harnessing bistability for directional propulsion of soft, untethered robots, Proc. Natl. Acad. Sci. U.S.A. **115**, 5698 (2018).
[35] S. Rudykh and K. Bertoldi, Stability of anisotropic magnetorheological elastomers in finite deformations: A micromechanical approach, J. Mech. Phys. Solids **61**, 949 (2013).
[36] A. Goshkoderia and S. Rudykh, Stability of magnetoactive composites with periodic microstructures undergoing finite strains in the presence of a magnetic field, Compos. Eng. **128**, 19 (2017).
[37] P. P. Castañeda and E. Galipeau, Homogenization-based constitutive models for magnetorheological elastomers at finite strain, J. Mech. Phys. Solids **59**, 194 (2011).
[38] E. Galipeau, S. Rudykh, G. deBotton, and P. Ponte Castañeda, Magnetoactive elastomers with periodic and random microstructures, Int. J. Solids Struct. **51**, 3012 (2014).
[39] K. Bertoldi and M. Gei, Instabilities in multilayered soft dielectrics, J. Mech. Phys. Solids **59**, 18 (2011).
[40] S. Rudykh, K. Bhattacharya, and G. deBotton, Multiscale instabilities in soft heterogeneous dielectrics, Proc. R. Soc. A **470**, 20130618 (2014).
[41] K. Danas and N. Triantafyllidis, Instability of a magnetoelastic layer resting on a non-magnetic substrate, J. Mech. Phys. Solids **69**, 67 (2014).
[42] E. Psarra, L. Bodelot, and K. Danas, Two-field surface pattern control via marginally stable magnetorheological elastomers, Soft Matter **13**, 6576 (2017).
[43] A. Dorfmann and R. Ogden, Nonlinear magnetoelastic deformations, Q. J. Mech. Appl. Math. **57**, 599 (2004).
[44] See Supplemental Material at http://link.aps.org/supplemental/10.1103/PhysRevLett.124.158002 for details about numerical modeling and instability analysis, and description of the experiment.
[45] Note that the normalization is not universal, and it is less appropriate for MAE composites with nonlinear magnetic materials with high filler volume fractions (that are not considered in this study).
[46] The average value is calculated by integrating the absolute value of the shear stress component over the domain of RVEs with the corresponding number ($N = 2$, 3, 4, and 5) of unit cells. The first and second terms of $\tilde{\sigma}_{yy}$ are dimensionless Maxwell and total Cauchy stress components, respectively.
[47] Note that the examples are shown in the postbuckling state of $\epsilon = 50\%$, and the buckling occurs prior to the strain level; the higher strain level is chosen for postbuckled examples to show the induced patterns in their well-developed state with visible magnitudes.
[48] To realize the periodic patterns with $N_p = 2$, 3, and 4, a MAE composite with $N = 24$ particles (including two-, three-, and four-particle periodicity) is used; for realization for the periodic pattern with $N_p = 5$, MAE composite with $N = 20$ particles is used. For illustration, we also include

the wavy and nonperiodic patterns in Fig. 2(h) from our simulation results with $N = 24$ particles.

[49] D. Kokkinis, M. Schaffner, and A. Studart, Multimaterial magnetically assisted 3d printing of composite materials, Nat. Commun. **6**, 8643 (2015).

[50] W. Man, M. Megens, P. J. Steinhardt, and P. M. Chaikin, Experimental measurement of the photonic properties of icosahedral quasicrystals, Nature (London) **436**, 993 (2005).

[51] D. Shechtman, I. Blech, D. Gratias, and J. W. Cahn, Metallic Phase with Long-Range Orientational Order and No Translational Symmetry, Phys. Rev. Lett. **53**, 1951 (1984).

[52] D. Levine and P. J. Steinhardt, Quasicrystals: A New Class of Ordered Structures, Phys. Rev. Lett. **53**, 2477 (1984).

[53] X. Zhao and Z. Suo, Theory of Dielectric Elastomers Capable of Giant Deformation of Actuation, Phys. Rev. Lett. **104**, 178302 (2010).

[54] G. Zurlo, M. Destrade, D. DeTommasi, and G. Puglisi, Catastrophic Thinning of Dielectric Elastomers, Phys. Rev. Lett. **118**, 078001 (2017).

[55] G. Zurlo and L. Truskinovsky, Printing Non-Euclidean Solids, Phys. Rev. Lett. **119**, 048001 (2017).